中國機械工程學刊第四十四卷第一期第 23~36 頁(民國一百一十二年)
Journal of the Chinese Society of Mechanical Engineers, Vol.44, No.1, pp 23~36 (2023)

Precise CD Measurement of Micro Grating Iinewidth Using Multi-view AFM Stitching Method

Liang-Chia Chen* , Nguyen Van Thai* and Bo-Ching He**

Keywords: critical dimension (CD); image registration; linewidth measurement; atomic force microscopy (AFM); image stitching.

ABSTRACT

This article presents a new critical dimension (CD) measuring method for nanoscale linewidth measurement of micro gratings employing an image stitching algorithm with AFM (atomic force microscope) multi-view scans. Due to the geometric constraints of AFM scanning, it has been considered a challenging and erroneous task to measure and reconstruct a micro grating using AFM since the AFM measuring tip in the scanning process cannot keep its measuring orientation well against both right-angle side walls of a grating simultaneously. To resolve this, a new strategy of using multi-view scanning with an image stitching algorithm for precise data fusion is presented. Some measurement experiments were conducted to verify the feasibility of the development. As confirmed by measured data, the measurement bias in measuring micro grating using AFM can be controlled at less than 1.0 nanometer for a grating with a linewidth of 820.1nm.

INTRODUCTION

Atomic force microscopy (AFM) is an instrument frequently employed to measure the 3-D surface profile of a grating with calibrated linewidth to study the measurement traceability of the standard target and standards. As we know, atomic force microscopy (AFM) (Heath, 2021; Giessibl, 2003; Lang, 2004) is one of the highly demanded instruments for the dimensions and is also often utilized for sensitive force measurement of critical dimensions of sub-nanometer measurement. The tip of AFM, in which the tip radius is within a range of 5-50 nm, can detect a single molecule of a measuring surface. The tip is often suspended with a soft spring, a cantilever beam. Due to the nanometer dimension of the AFM tip radius, it probes a small depth of view and thus gives high sensitivity to small height changes. The cantilever scanned over the surface with the extremely short distance between tip and surface is of the order of 0.2 - 10.0 nm. Therefore, AFM is also extensively used for 3-D measurement of critical dimensions. However, due to the geometric constraints of AFM scanning, it has been an erroneous task to measure and reconstruct a micro grating using AFM. In traditional scanning, an AFM measuring tip (Vekinis, 2020; Canet-Ferrer, 2014) cannot continually keep its measuring orientation well against both of the vertical-angle side walls of a grating simultaneously. The 3-D point clouds scanned from a single-view AFM scan may often possess unacceptable measured errors due to the above tip-side effects. When the tip scanning direction is inclined with the surface normal for over 30 degrees, the measured result often deteriorates severely due to an undesired increase of the tip side effect. Therefore, a new measurement strategy employing an iterative closest point (ICP) stitching algorithm with multi-view AFM scans is proposed to reconstruct the critical linewidth of a grating (Bai et al., 2021; Kleinknecht, 1980).

In the proposed method, image registration plays an important role in determining the measurement accuracy of grating linewidth measurement. Fundamentally, the ICP algorithm has been used widely for image registration, and it was first introduced by Besl (Besl et al., 1992). In his work, a 6-degree-of-freedom image registration with unknown data correspondences heavily depends on the model shape defined for the unknown transformation, which iteratively searches for the closest distance between two sets of point clouds, and the merit function may converge to local minima when the signal to noise ratio (SNR) of the data matching is sound. Meanwhile, Chen (Chen et at., 1992) developed an image registration approach for complex objects by minimizing the matching distance derived from the 3D geometric shape of objects without any point-to-point matching.

Paper Received October, 2022. Revised December, 2022. Accepted December, 2022. Author for Correspondence: Liang-Chia Chen, lchen@ntu.edu.tw

* *Professor and his PhD student, Department of Mechanical Engineering, National Taiwan University, , No.1, Sec. 4, Roosevelt Road, Taipei 10617, Taiwan, R.O.C*

** *Research fellow, Center of Measurement Standards, Industrial Technology Research Institute, Hsinchu 30011, Taiwan, R.O.C*

However, the object's shape information may be unknown in most real cases. In 1994, Zhang extended ICP to include freeform curves and surfaces (Zhang, 1994). An algorithm was proposed to iteratively match the points in one set to the closest point in the other without imposing a constraint on the shape of objects and using any pre-processing operation. These ICP algorithms generally work well when each matching point has its correct corresponding point. However, the ICP algorithm may be affected by outliers such as measured noises or occlusion.

In 1995, Masuda (Masuda, 1995) proposed a registration method to remove undesired measured noises in point clouds. In 1997, Dorai developed an optimal weighted least-squares framework to minimize the matching distance (Dorai, 1997) by deriving a minimum variance estimator to estimate the transformation parameters more reliably. The proposed minimum variance estimator was proved to be more effective than other unweighted distance criteria proposed earlier. Based on a similar concept of using weighted distance criterion, another method called Iterative closest points using invariant features (ICPIF) (Sharp et al., 2002) selects the nearest-neighbor correspondences according to a distance metric which is a scaled sum of the positional and feature distance. In 2003, Huber presented a registration method that doesn't require using a hand or any external positioning device (Huber, 2003). His work automatically registers multiple rigid 3-D data sets, called multi-view surface matching, and requires fewer scans for a measured object. The multi-view surface matching divides the data registration problem into two stages: a local registration phase and a global registration phase. These two registration phases involve estimating rigid transformation in two stages to reduce the degree of complexity in 6-degree of freedom of image matching.

To overcome the non-linearity of the registration process, Fitzgibbon introduced a new method for directly minimizing the registration error by using non-linear optimization (Fitzgibbon et al., 2003). Surprisingly, the speed of the proposed technique is comparable with the speed of the ICP algorithm. Meanwhile, Pottmann presented an alternative concept of the ICP algorithm using instantons kinematics and local quadratic approximations to the least-squares distance function (Pottmann et al., 2004). In addition, this method also has the advantage of fast convergence behavior compared to other ICP algorithms. One year later, Gruen proposed a method called least-squares 3D surface matching to match one or more 3D point clouds to a 3D template surface and minimizes the sum of the least-squares of the Euclidean distances between the matching surfaces (Gruen et al. 2005). Akca gave an extension of Gruen's method in 2007 (Akca, 2007), in which additional attribute information was considered. However, all the above methods are adequate to minimize the least-squares matching distance to some degree. However, these are based on either some assumptions or geometric constraints, which may not be practical for a more generic problem to be handled in a non-linear model approximation.

One of the significant constraints in processing 3-D point clouds acquired using an AFM is the significant data size of points clouds, which could easily lead to substantial computation time in the image registration process. In addition, huge point clouds could consume excessive computational memory, so the non-linear least-squares approximation in the 6-degree-of-freedom model estimation could lead to a divergent optimization problem. To reduce the computational time and improve the convergence behavior and robustness of alignment iterations in automatic 3-D data registration, the resolution of clouds should be strategically reduced first. The raw point clouds are usually filtered appropriately based on the normal vectors, mean distances, and numbers in the neighboring structure of the point clouds, so the measured noises, such as outliers, can be effectively filtered and removed from the main structure of the topological shape of the measured surface. 6-degree-of-freedom model transformation estimation can be implemented based on the filtered clouds. To achieve this, a procedure of linewidth measurement for two point-cloud datasets underlying alignment is developed. Generally, the ICP algorithm taken in the procedure can iterate the estimation of the best model from the neighboring structure points between individual 3D datasets (or called images) obtained from different AFM scans and determines the best closest point for computing the best 6-degree-of-freedom transformation that minimizes deviations between the two datasets of neighboring structure point pairs. The proposed strategy uses the ICP to find the best 6-degree-of-freedom model transformation between multi-view scans of AFM measurement on gratings.

The article is organized in the following sequence. Section 2 introduces the concept of multi-view AFM scanning. Section 3 describes for data representation used in the proposed point-cloud processing procedure. Following this, Section 4 overviews the global algorithm for reconstructing the reconstructed surface from multi-view AFM scans. The key issues are addressed in the pre-processing data algorithm for the measured point clouds generated from AFM scans and the data filtration of measured noise (outliers) in the clouds. More importantly, a novel algorithm for the best nearest-neighboring search that can significantly reduce computation time for searching the best neighboring point in a set of point clouds is elaborated in Section 5. According to the reconstructed surface, a cross-section is measured at a specified height to calculate the grating linewidth as a critical dimension (CD). In addition, this section also proposes an algorithm for ICP-based point cloud

registration. Section 6 illustrates measured results in five case studies. Finally, some conclusions are summarized in Section 7.

MULTI-VIEW AFM SCANNING

As illustrated in Figure 1, the grating is scanned by multi-view AFM scanning, so the tip approaching direction can be kept a designed best titling angle with the surface normal of the measured surface region. Figures show the proposed multi-view AFM scanning strategy in micro grating surface measurement and reconstruction, in which the flat top surface of the grating can be scanned and used for image overlapping by both sides of the AFM scan having two different scanning orientations shown in Fig. 1. For each grating measurement, the micro grating is orientated at least four various viewpoints from the measuring AFM tip viewpoint; thus the grating profile can be desirably separated into multiple detecting surface regions for best surface measurement and reconstruction. By doing this, individual detecting surfaces with appropriately overlapping neighboring regions can be scanned and measured seamlessly for further 3-D image registration and surface reconstruction.

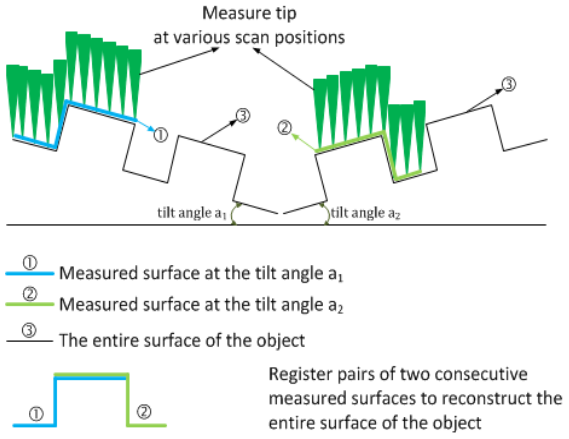

Fig. 1 Proposed multi-view AFM scanning strategy in micro grating surface measurement and reconstruction, in which the flat top surface of the grating can be scanned and used for image overlapping by both sides of AFM scan having two different scanning orientations shown.

DATA REPRESENTATION

A collection of 3-D data points acquires a discrete representation of the 3-D profile of the measured sample. A point Pi, described by $\{x_i, y_i, z_i\}$, is an elementary representation unit in a three-dimensional (3-D) Euclidean space. A collection of 3-D points referred to as a cloud structure P. Every point Pi is given concerning a fixed coordinate system. In most cases, the coordinate system defined here originates in the sensing device used to acquire the data. Hence, we can estimate a point *Pi* as the distance on the three defined coordinate axes between the acquisition viewpoint and the surface from which the point has been measured.

RECONSTRUCTION OF THE GLOBAL SURFACE OF MULTI-VIEW AFM SCANS

Each area of the surface is scanned by more than one viewpoint. In the proposed method, the micro grating is orientated at least four different viewpoints from the measuring AFM tip viewpoint for each grating measurement. Thus, the grating profile can be desirably separated into multiple detecting surface regions for best surface measurement and reconstruction. The registration algorithm then registers these scans to obtain the rigid transformation matrix. As shown in Figure 2, the proposed registration algorithm is illustrated by a flow chart diagram, including several essential steps to be introduced below.

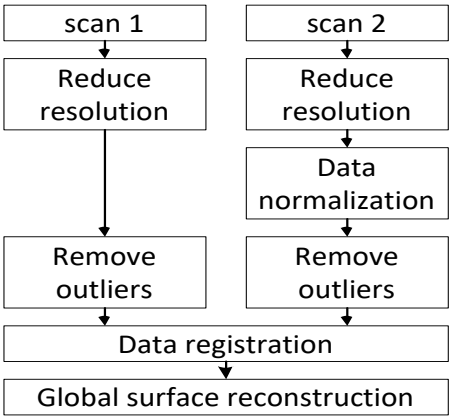

Fig. 2 Flowchart of the global surface reconstruction algorithm for multi-view AFM scans.

Reduction of resolution for AFM scans

Each AFM scan may consist of many points in a measured cloud, e.g., 4096 x 4096 for more than 16 mega points for only an AFM scan. The direct computation on these point clouds can be significantly massive in the registration processing and may lead to computation instability, especially in the global optimization processing. It could also be significantly time-consuming for computation which could easily lead to computing instability. Therefore, the size of clouds should be initially reduced in its resolution before a fine model estimation is implemented.

Normalization of data

Before the ICP's registration, since the shifting between two AFM scans can be performed in the second scan by orientating the grating with a nominal angle, two data sets can be initially registered to their first orientation. An accurate rotator controls the

second scan with an adequate angle adjustment, such as 180°.

Removal of outliers

In addition, the acquired data from AFM scans may possess some measured errors incurred by potential measurement uncertainties in AFM scan that may induce sparse outliers. The unacceptable measured errors may be incurred since potential tip side effects could exist in the scanning process. Moreover, the removal of outliers helps reduce processing time since the cloud size is reduced accordingly. In the development, three kinds of outlier removal methods have been integrated into the procedure shown in Fig. 3 to eliminate outliers. In the process, three data filtering principles based on normal vectors, mean distance, and the number of neighboring points are synthesized and integrated into the filtering process to achieve the best noise filtration.

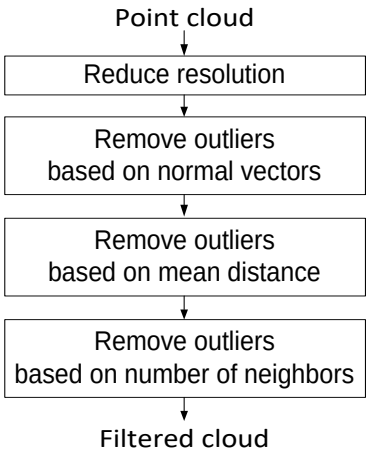

Fig. 3 Flowchart of the outlier removal algorithm.

As the first outlier filtering, $|\vec{n} \cdot \vec{s}|$, named by scanning alignment quality (SAQ), where $\vec{n}$ is the normal vector at the query point. Meanwhile, $\vec{s}$, called the scanning vector, is calculated for all of points in the cloud. Points having a high SAQ are retained, otherwise eliminated. Fig. 4 shows the first outlier filtering based on normal vectors.

As the second outlier filtering, the filter is developed to remove undesirable outliers, which have excessive measured errors, employs a statistical analysis on each point's neighbors by assuming a Gaussian distribution of the spatial data distribution with a mean and a preset standard deviation. All points with their mean distances outside the present standard deviation are considered outliers and removed from the dataset.

The mean deviation from each point to all its neighbors in the cloud is calculated as follows:

$$\mu_i = \frac{1}{N}\sum_{k=1}^{N}\|p_k - q_i\| \quad (1)$$

where $p_k, k = 1 \sim N$, are neighbors, and N is the number of neighbors at the query point q_i in the cloud, meanwhile $\|p_k - q_i\|$ is the Euclidean distance between point q_i and point p_k.

With a mean and a standard deviation, all points having their mean distance outside a specific interval are considered outliers since they are removed from the cloud. Alternately, as the third outlier filtering, the point number of neighbors around a query point in the cloud is counted. The query point is considered an outlier when the counted number is less than an appropriate preset threshold.

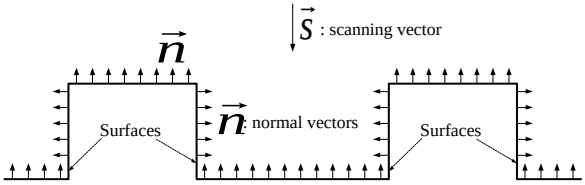

Fig. 4. The first outlier filtering based on normal vectors.

Estimation of rigid-body transformation

Let Ps be the source point set, and Pt is the target point set [Besl, 1992; Chen, 1992].

$$P_s = \{\vec{p}_s\} \quad (2)$$

$$P_t = \{\vec{p}_t\} \quad (3)$$

where P_s consists of the 3-D points in the first AFM scan, while P_t consists of the 3-D points in the second AFM scan. The rigid transformation, RT^k, and the mean square error, MSE_k, are then calculated at the k^{th} iteration. MSE_k is compared with an appropriate preset threshold so that the best transformation can be iteratively approached. Fig. 5 illustrates the flowchart of the rigid transformation estimate algorithm developed for the data registration based on the ICP principle.

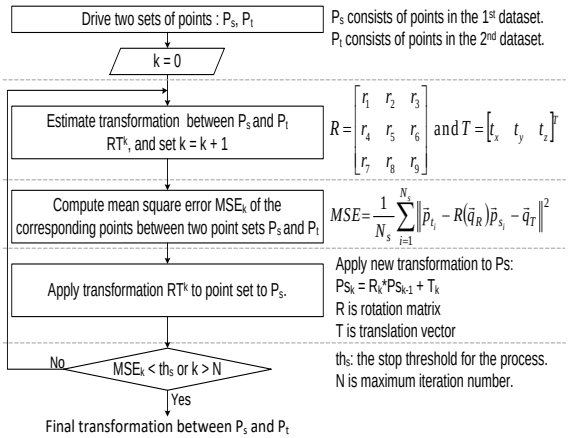

Fig. 5 Flow chart diagram of the developed rigid transformation estimation algorithm.

The "center of mass" of these point sets are given by:

$$\vec{\mu}_s = \frac{1}{N_s}\sum_{i=1}^{N_s}\vec{p}_s \tag{4}$$

$$\vec{\mu}_t = \frac{1}{N_t}\sum_{i=1}^{N_t}\vec{p}_t \tag{5}$$

The cross-covariance matrix between P_s and P_t are determined as:

$$\Sigma_{st} = \frac{1}{N_s}\sum_{i=1}^{N_s}\left[\left(\vec{p}_{s_i} - \vec{\mu}_s\right)\left(\vec{p}_{t_i} - \vec{\mu}_t\right)^T\right] \tag{6}$$

A symmetric 4 x 4 matrix is formed as follows:

$$Q(\Sigma_{st}) = \begin{bmatrix} tr(\Sigma_{st}) & \Delta^T \\ \Delta & \Sigma_{st} + \Sigma_{st}^T - tr(\Sigma_{st})I_3 \end{bmatrix} \tag{7}$$

where $\Delta = [A_{23} \quad A_{31} \quad A_{12}]$ and $A_{if} = (\Sigma_{st} - \Sigma_{st}^T)_{ij}$

$I_3 = \begin{bmatrix} 1 & 0 & 0 \\ 0 & 1 & 0 \\ 0 & 0 & 1 \end{bmatrix}$: 3×3 identity matrix

The unit eigenvector corresponding to the maximum eigenvalue of the matrix $Q(\Sigma_{st})$ is given by

$$\vec{q}_R = [q_0 \quad q_1 \quad q_2 \quad q_3]^T \tag{8}$$

The optimal rotation matrix between the source and target point set is estimated by:

$$R = \begin{bmatrix} q_0^2+q_1^2-q_2^2-q_3^2 & 2(q_1q_2-q_0q_3) & 2(q_1q_3+q_0q_2) \\ 2(q_1q_2+q_0q_3) & q_0^2+q_2^2-q_1^2-q_3^2 & 2(q_2q_3-q_0q_1) \\ 2(q_1q_3-q_0q_2) & 2(q_2q_3+q_0q_1) & q_0^2+q_3^2-q_1^2-q_2^2 \end{bmatrix} \tag{9}$$

The optimal translation vector between the source and target point set is given by

$$\vec{q}_T = \vec{\mu}_t - R(\vec{q}_R)\vec{\mu}_s \tag{10}$$

where $\vec{q}_T = [q_4 \quad q_5 \quad q_6]^T$

The iteration is initialized by setting $\vec{q}_{T_0} = [0 \quad 0 \quad 0]^T$.

The mean squares objective function to be minimized is expressed as:

$$MSE_k = \frac{1}{N_s}\sum_{i=1}^{N_s}\left\|\vec{p}_{t_i} - R(\vec{q}_R)\vec{p}_{s_i} - \vec{q}_T\right\|^2 \tag{11}$$

Novel algorithm of the nearest-neighbor search for large datasets

Processing normal vectors at query points in the cloud could be an expensive cost function. In particular, the neighboring search is a time-consuming process. Fortunately, some database computation techniques have been developed which can overcome the problem of nearest-neighbor search, such as kd-tree (Bentley, 1975; Sproull, 1991), quad-tree (Finkel, 1974), octree (Jackins, 1980), vp-tree (Yianilos, 1993), and ball tree (Liu, 2006; Omohundro, 1989). The proposed method introduces a new algorithm to structurize and search for large datasets of AFM-scanned 3-D images, thus significantly reducing computation time in a neighboring search.

The nearest-neighbor (NN) problem is here considered in three-dimensional Euclidean space. The data points are first structuralized as a tree which contains a root, some nodes, and leaves. Each node has at least one child and a maximum number of 23 children. In addition, a strategy for nearest-neighbor search in the tree has also been developed. The goal is to search neighbors efficiently around a given query point in the datasets. Let a data point P contain 24 unorganized points, as shown in Fig. 6. The boundary and center of data points are determined based on their minimum and maximum for x-components and y-components. This center plays a role as the root of a tree. Since points are partitioned into 4 possible sub-partitions, assuming that the number of points in each sub-partition should not be more than 4 points, 4 child nodes can be generated with boundaries corresponding to each sub-partition. A recursive process repeats until sub-partitions contain a maximum of 4 points which play a role as leaves. Fig. 7 shows the structuralized tree of this example data.

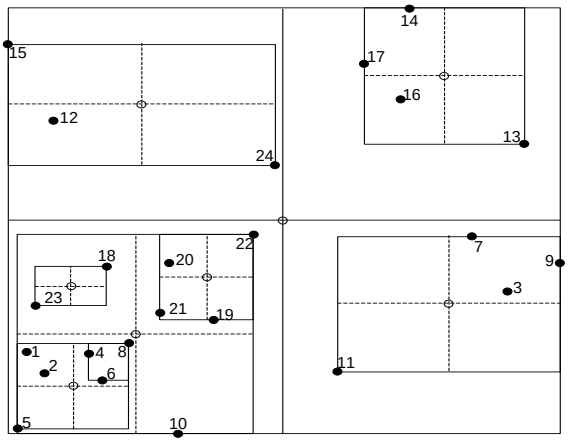

Fig. 6 Distribution of unorganized data points and their partitions.

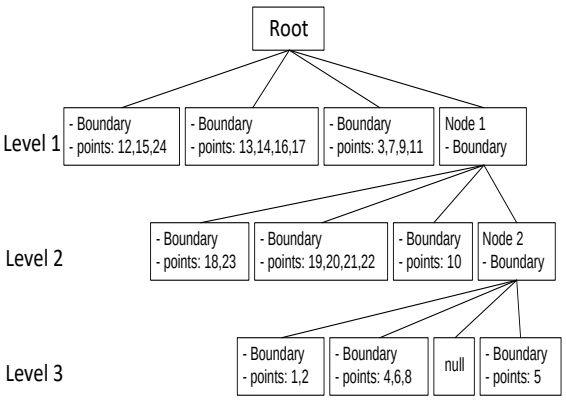

Fig. 7 Structuralized tree in a neighboring search.

The strategy for nearest-neighbor search is defined based on the constructed tree. Assuming a query is given, as shown in Fig. 8, the search circle is collated at level 1 to find the overlaps between the circle and

boundaries. Overlap is identified at Node 1. Recursive collate at level 2, the overlap is found at the first leave; thus, two neighbors have been found using the Euclidean distance algorithm.

EXPERIMENTAL RESULTS AND ANALYSIS

Several measured tests were performed with multi-view AFM scans on micro gratings to evaluate the feasibility of the proposed method for AFM linewidth measurement. Experiments were performed by conducting the following five required procedures: (1) data resolution reduction of measured point clouds from AFM scans; (2) removal of outliers for measured point clouds; (3) registration of measured point clouds; (4) AFM linewidth measurement; (5) comparison of linewidth measurement between AFM and SEM.

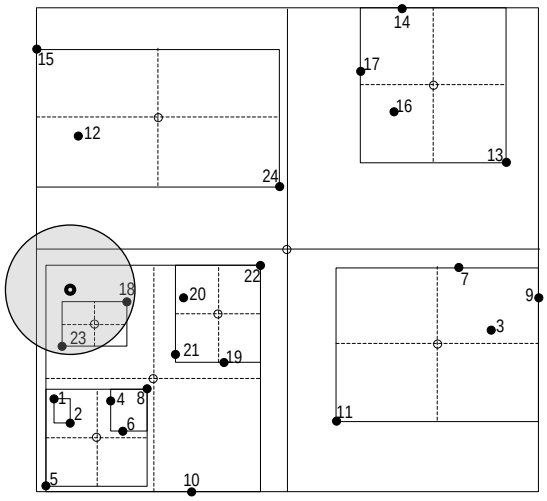

Fig. 8 The given query point for NN search within a radius.

Data resolution reduction of measured point clouds from AFM scans

The 3-D measured image of each scan can be first outputted using NanoScope Analysis and saved as an image. The AFM employed in this research is *Bruker Dimension Icon* with its calibrated measurement accuracy of X-Y Position noise less than 0.15 nm and RMS Z sensor noise level less than 35 pm RMS.

Pairs of measured data were extracted from text files, they were then pre-processed by reducing point resolution to significantly reduce the cloud size. To investigate this study case, four pairs of measured AFM scans were extracted. Fig. 9 shows clouds and scaled clouds for Pair 1 of the AFM scans by 512×512 pixels. The number of points extracted from AFM scans for Pair 1 was 262,144 points. Meanwhile, the number of points for its scaled point clouds was calculated by an appropriate scale factor σ, in which the scale was 5. The retained points are points that have both "index-row mod σ" and "index-column mod σ" all equal to zero as shown in Fig. 10.

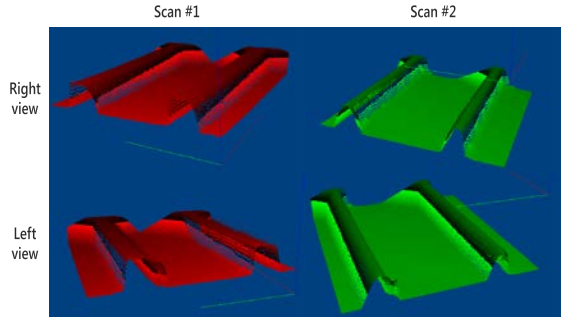

(a)

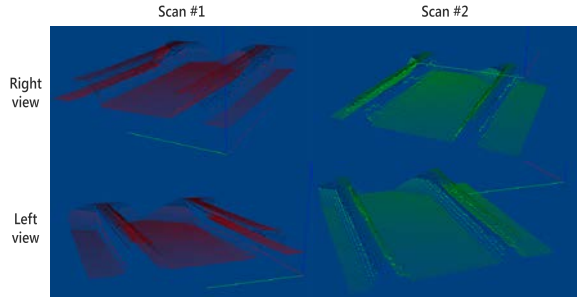

(b)

Fig. 9 Four pairs of measured AFM scans: (a) clouds were formed from Pair 1 of the AFM scans. The number of extracted points was 262,144 points for each cloud. (b) The clouds of Pair 1 were then scaled by a factor of 5; hence, the number of retained points was 10,609 points for each cloud.

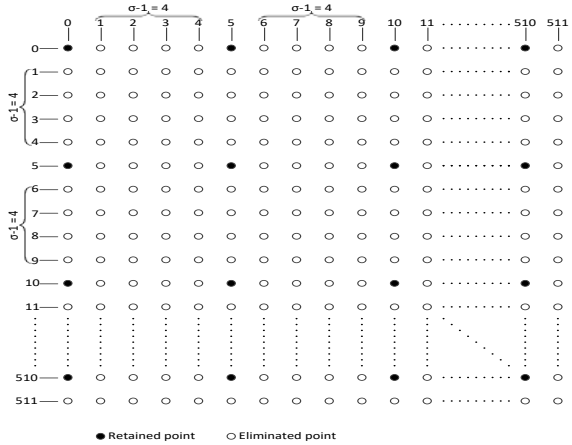

Fig. 10 Scaling a cloud of 512×512 points by a scale factor σ = 5.

Fig. 11 shows clouds and scaled clouds for the AFM scans of Pairs 2, 3, and 4. Parameters and settings for extraction and reduction for measured point clouds generated from AFM scans as shown in Table 1. The number of points extracted from AFM scans for Pair 2, 3, and 4 was 262,144, 262,144 (512×512 pixels of AFM scans), and 524,288 (512×1024 pixels of AFM scans) points, respectively. Meanwhile, the number of points for the scaled point clouds was 10,609 points for Pairs 2 and 3 by a scale factor 5 and 6,498 points for Pair 4 by a scale factor of 9.

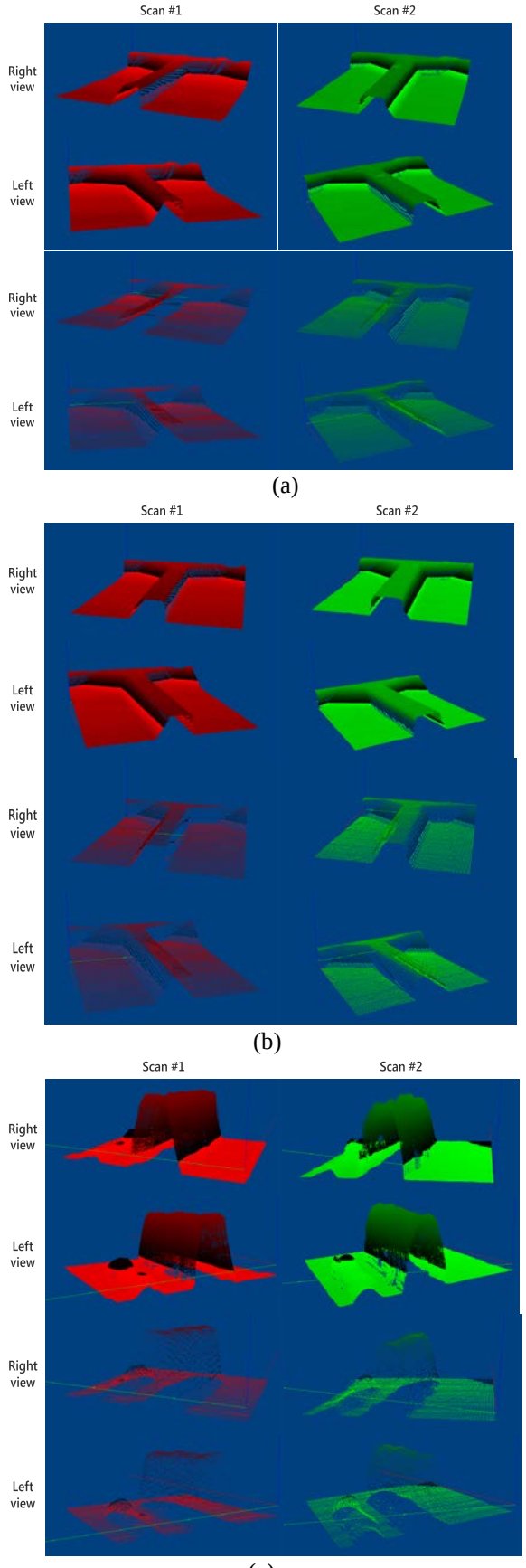

Fig. 11 Point clouds and scaled point clouds extracted from the pair 2 (a), 3 (b), and 4 (c) of the AFM scans.

Table 1. Parameters and settings for AFM scan to extract and reduce measured point clouds.

AFM scans		*s* μm	*R* nm	*N* (pts)	*f*	*Dev* (nm)	P_F (pts)
Pair	*scan*						
1	1st	1.99	5	15	2	15.54	6,663
	2nd	1.99	5	15	2	15.54	7,707
2	1st	2.03	5	15	2	19.82	8,451
	2nd	2.00	5	15	2	15.62	8,678
3	1st	2.00	5	15	2	15.62	8,641
	2nd	1.88	5	15	2	14.68	8,715
4	1st	0.45	5	15	1	10.62	6,308
	2nd	0.45	5	15	1	10.61	6,292

N: threshold of the number of neighbors for outlier removal
r: standard deviation of the radius for a neighbour search around a query point in the cloud.
P_F: the filtered point cloud using the proposed method.

Table 1 *Set parameters and results for outlier removal.*

AFM scans		*W* (pixel)	*H* (pixel)	σ	P_M (point)	P_S (point)
pair	*scan*					
1	1st	512	512	5	262,144	10,609
	2nd	512	512	5	262,144	10,609
2	1st	512	512	5	262,144	10,609
	2nd	512	512	5	262,144	10,609
3	1st	512	512	5	262,144	10,609
	2nd	512	512	5	262,144	10,609
4	1st	512	1024	9	524,288	6,498
	2nd	512	1024	9	524,288	6,498

P_M: the measured point cloud was extracted from the AFM scan.
P_S: the scaled point cloud by a scale factor σ.
w, *h* present the width and height of AFM scans, respectively.

Removal of outliers for measured point clouds

Outliers were filtered based on the following properties: the first was the normal vector at each query point, the second was the mean distance from each point in the cloud to all its neighbors, and the third was the number of neighbors at each query point. Consequently, the clouds' size was reduced significantly, thus reducing the processing time in the registration step. The standard deviation for outlier removal was calculated by

$$Dev = \frac{s\times\left(\frac{1}{w}+\frac{1}{h}\right)\times(\sigma-1)}{f} \qquad (12)$$

where *s* denotes the scan size of the AFM scan; *f* is an adjustable factor for the standard deviation.

Outliers are considered noises that contribute negatively to the data registration process. These outliers have been rejected to guarantee convergence and

accuracy in alignment iterations, and the processed data only retain good points. In addition, the number of points can be reduced by up to 30% of the original data size. This operation can effectively reduce the processing time in the registration process. However, the computation cost for rejecting outliers may also be expensive. The setting of parameters for outlier removal, such as the number of neighbors and standard deviation to confirm a querying point, is important and can significantly affect the computation time and the number of retained points. Table 2 shows the necessary parameters for outlier removal using the proposed method and corresponding experimental results. Fig. 12 shows the visualization of these measured results.

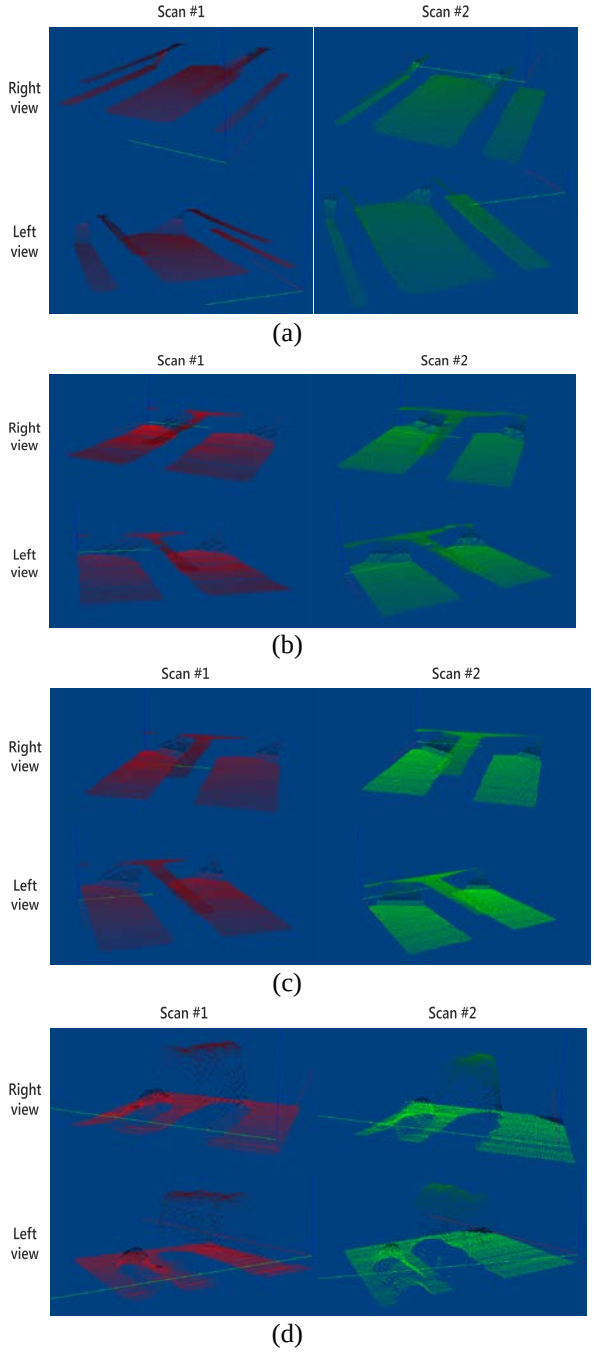

Fig. 12 Filtered point clouds were obtained by applying the proposed method for outlier removal for (a) Pair 1, (b) Pair 2, (c) Pair 3, and (d) Pair 4.

Removal of outliers for measured point clouds

In the experiments, the measured point clouds were first filtered using the proposed method to scale down the measured point clouds to a computation-friendly level and remove data outliers. Experimentally, the size of clouds was kept to an appropriate number, such as 10,000 points, to guarantee convergence in the image registration process. In the experimental tests, at least three cross-sections were selected at three different positions along the horizontal axis to evaluate the registration accuracy for data pairs. Figs 13, 14, 15, and 16 show the results of data registration for Pairs 1, 2, 3, and 4 based on their corresponding filtered point clouds, respectively.

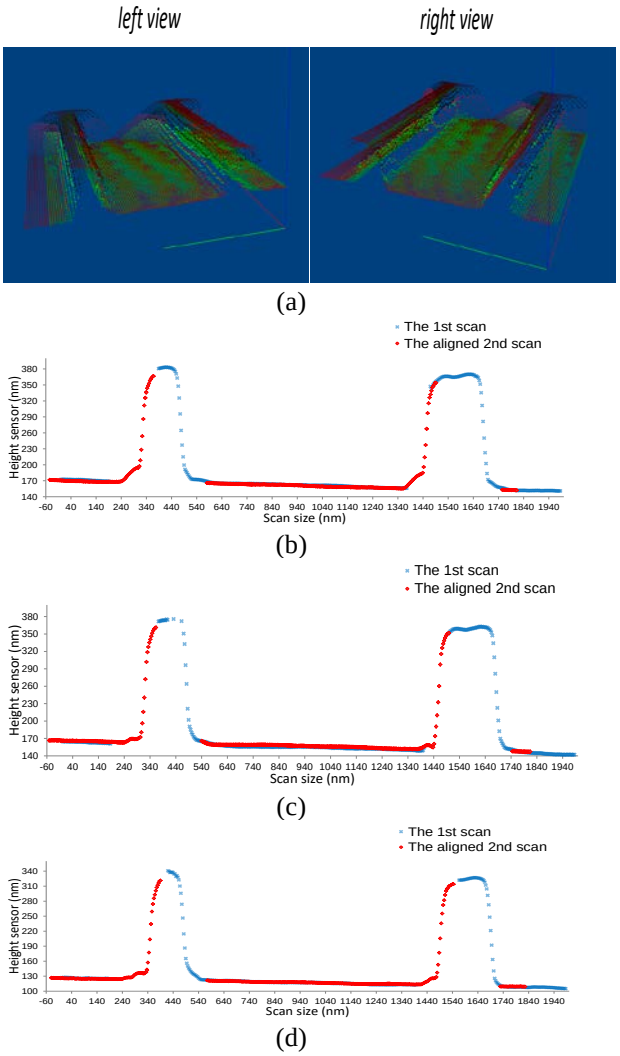

Fig. 13 Measured results of Pair 1: (a) Visualization of the result for registration of Pair 1 based on filtered point clouds for the first scan, 6,663 points, and the second scan, 7,707 points. Cross-sections were picked up at Line 65 (b), 100 (c), and 390 (d), respectively.

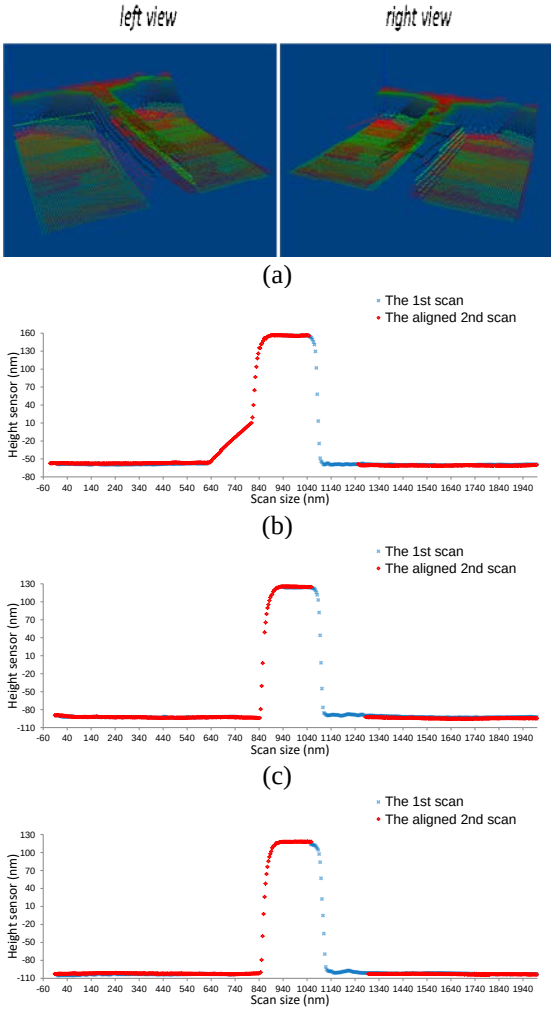

Fig. 14 Measured results of Pair 2: (a) Visualization of the result for registration of Pair 2 based on filtered point clouds for the first scan, 8,451 points, and the second scan, 8,678 points. Cross-sections were picked up at Line 133 (b), 300 (c), and 350 (d), respectively.

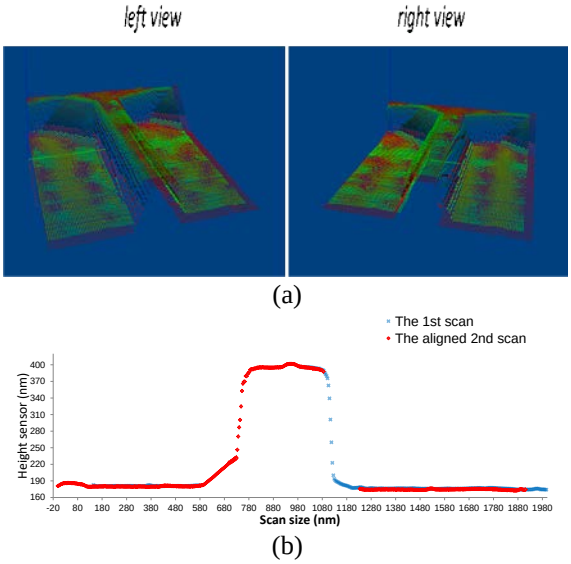

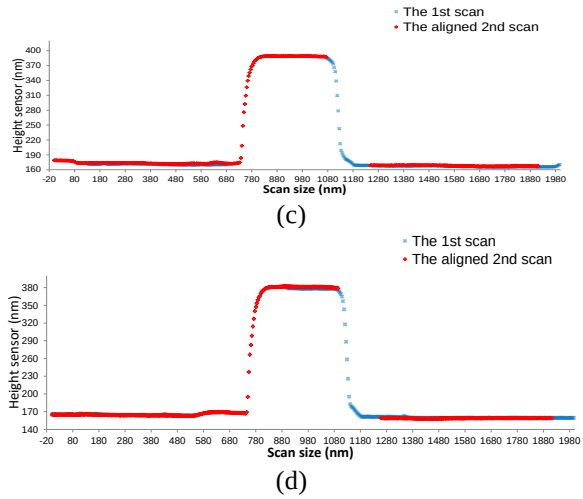

Fig. 15 Measured results of Pair 3: (a) Visualization of the result for registration of Pair 3 based on filtered point clouds for the first scan, 8,641 points, and the second scan, 8,715 points. Cross-sections were picked up at Lines 130 (b), 200 (c) and 300 (d), respectively.

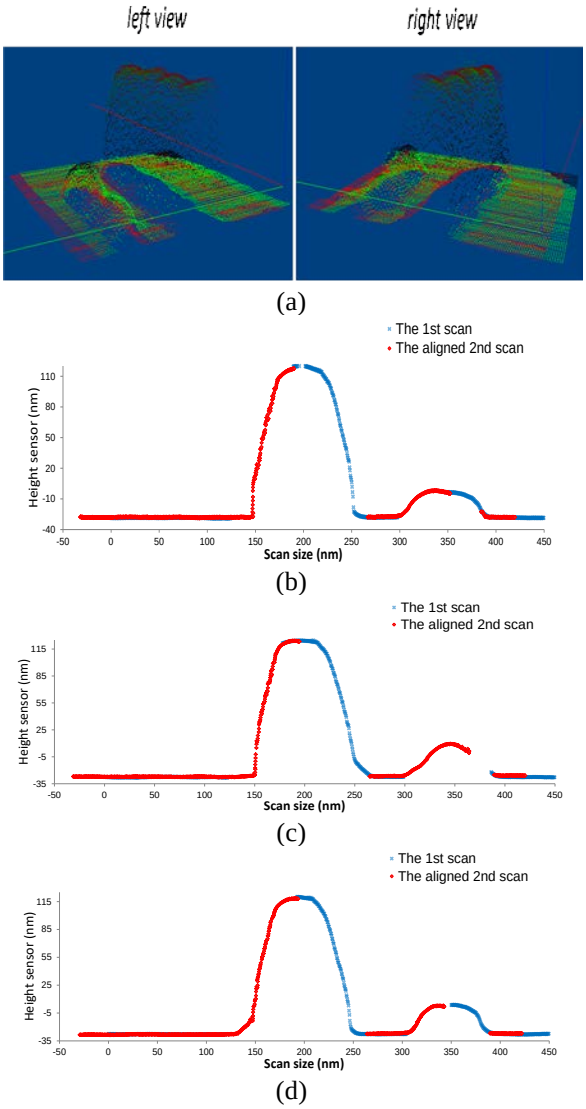

Fig. 16 Measured results of Pair 4: (a) Visualization of the result for registration of Pair 4 based on filtered point clouds for the first scan, 6,308 points, and the second scan, 6,292 points. Three cross-sections were picked up at Line 166 (b), 206 (c), and 300 (d), respectively.

AFM linewidth measurement

Fig. 17 shows the measured results of the AFM linewidth measurements at several different positions along the horizontal axis in 4 case studies. The proposed method can measure CDs of cases 1-4. As demonstrated, the existing difficulty of AFM measurement on grating linewidth described in the Introduction can be effectively addressed.

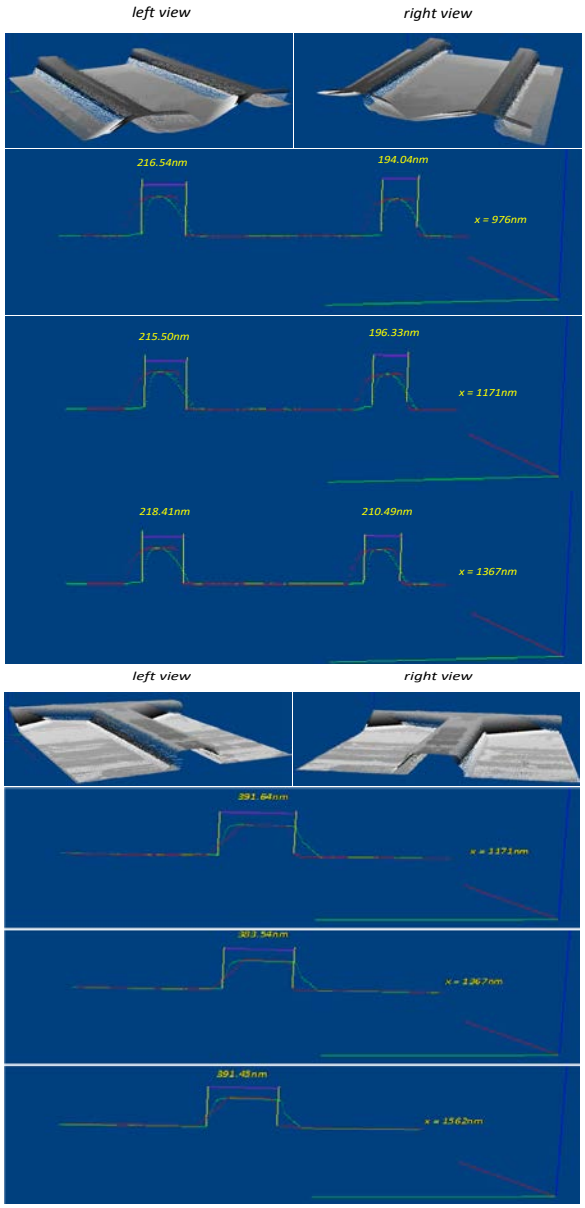

Fig. 17 Three cross-sections were measured and evaluated for linewidth measurements in 4 case studies.

EVALUATION AND DISCUSSION ON MEASURED RESULTS

Several dimensional comparisons between the pre-calibrated SEM, TEM cross-section dimensions, and the reconstructed 3-D data by the developed method were used to evaluate the measurement accuracy of the proposed methodology in reconstructing the measured target. Since the linewidth varies with the grating height, a specific height is assigned in the measurement verification. Our test selected a specified height position of 120 nm from the defined bottom line. From the measurement test, Fig. 18 illustrates the cross section measured at the specified height position for dimension comparison; the measured values were 104.5 and 62.5 nm by AFM and SEM, respectively. From our investigation, it was concluded that the bias is mainly incurred by the image dilation of the grating surface with the tip's diameter in AFM measurement, even when the effect of tip shape interference has been effectively minimized by the proposed multi-view scans method (Dahlen, 2006). Thus, the tip's diameter was estimated by SEM image in the study, and then the value of 42.0 nm was obtained. Finally, the actual linewidth of the tested micro grating measured by AFM should be compensated for the tip's radius. The linewidth of the AFM measurement was 62.5 nm.

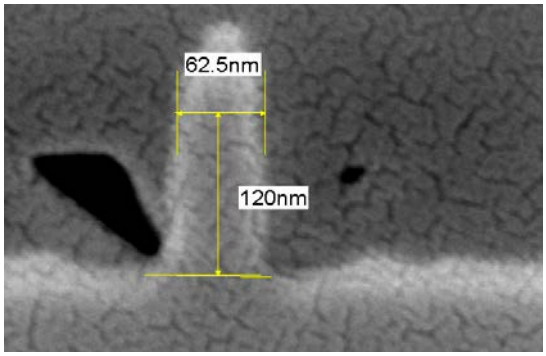

(a)

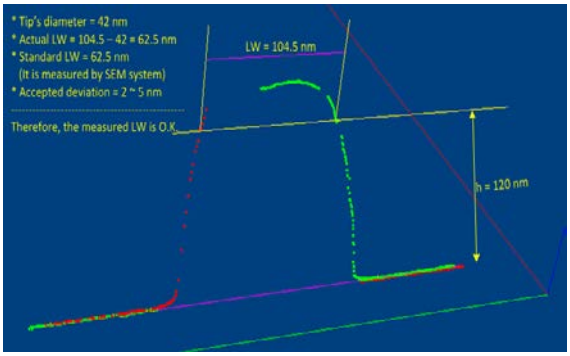

(b)

Fig. 18 The measured result of linewidth measurement of the micro grating by (a) SEM and (b) AFM, respectively, in which the measured tip's diameter of the AFM system was estimated to be 42.0 nm.

Fig. 19 shows the results of linewidth measured by AFM and TEM. The tip's diameter was measured and confirmed to be 29.03 nm. In this measured experiment, by AFM measurement, five cross sections have been established to calculate five results of linewidth: 844.7 nm, 858.1 nm, 853.7 nm, 843.2 nm, and 849.2 nm for cross sections at Lines 100, 150, 200, 400, and 450, respectively. The actual linewidth was calculated by averaging

$$lw = \frac{1}{N}\sum_{i=1}^{N} l_i \qquad (13)$$

where N denotes the number of cross sections; meanwhile, l_i represents the measured linewidth after subtracting from the tip's diameter.

The actual linewidth measured by AFM in this experiment was 820.8nm. Meanwhile, the result of TEM for this sample (800nm) was 820.1nm. Experimentally, the linewidths measured by AFM and TEM were similar. It is confirmed that the measurement bias of the linewidth measurement of the tested micro grating can be controlled to be within 1 nanometre.

The measurement accuracy and precision of the measurement of micro grating linewidth using the proposed multi-view AFM stitching method can be affected by a couple of important uncertainty factors of the image stitching algorithm. First, the signal-to-noise ratio (SNR) of the AFM-measured data is the major factor to affect the performance of the image stitching algorithm. The quality of AFM scanned point cloud from test samples can directly affect the measured bias and precision of the surface stitching result since the ICP performance greatly relies on the soundness of the stitched data. The acquired data from AFM scans may possess some measured errors incurred by potential measurement uncertainties in AFM scan that may induce sparse outliers. The unacceptable measured errors may be incurred since AFM's potential tip side effects could exist in the scanning process. Moreover, the removal of outliers helps reduce processing time since the cloud size is reduced accordingly. Thus, to ensure the high quality of the input measured surface data from AFM, an outlier removal algorithm was developed and used to filter out unacceptable measured noises and enhance the SNR of the input data for the image stitching algorithm. In addition to the data quality, the performance of the image stitching algorithm may also affect the final result. A novel algorithm based on the nearest-neighbor search for large datasets was developed to ensure good convergence and efficiency of the iterative stitching process. With these developed algorithms, image-stitching uncertainty can be minimized. As confirmed by measured data, the measurement bias in measuring micro grating using AFM can be controlled at less than 1.0 nanometer for a grating with a linewidth of 820.1 nm.

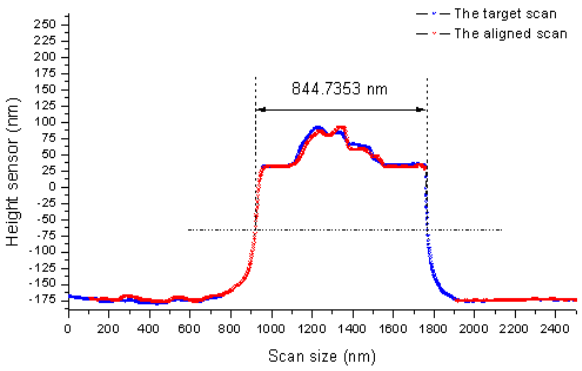

(a)

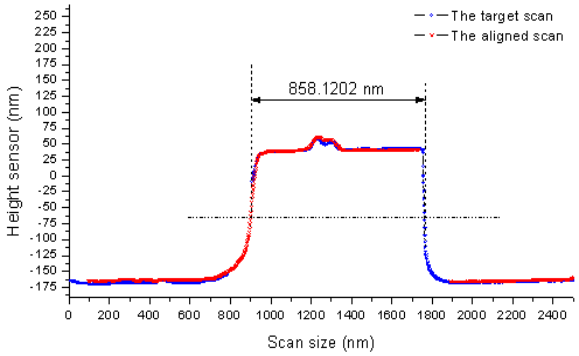

(b)

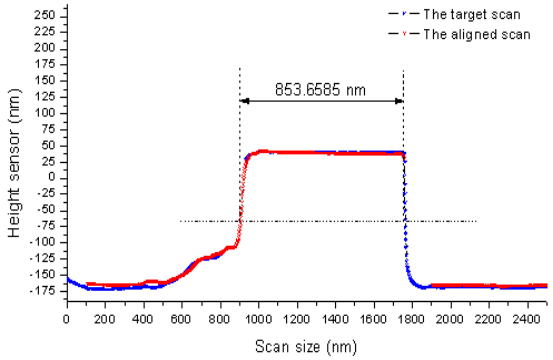

(c)

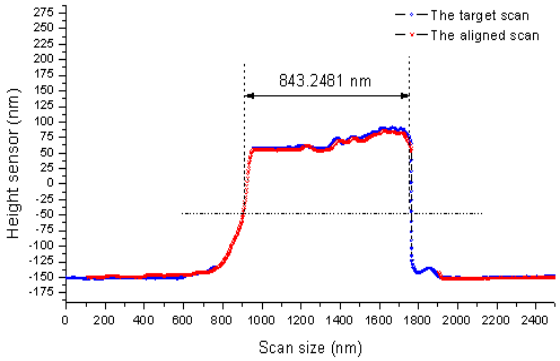

(d)

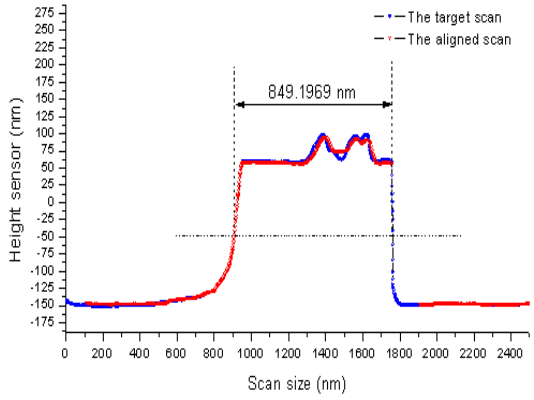

(e)

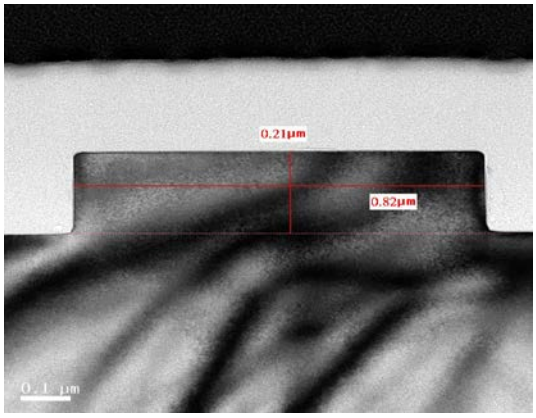

(f)

Fig. 19 Grating linewidth measured by AFM and TEM for a tested sample with a nominal size of 800 nm. (a), (b), (c), (d) and (e) are AFM linewidths measured by the cross sections at line 100, 150, 200, 400 and 450, respectively; (f) TEM linewidth.

CONCLUSIONS

In the study, a linewidth measurement methodology by stitching multi-view AFM scans with the proposed data processing procedures has been effectively developed for surface profile reconstruction of accurate CD measurement of micro gratings. The reconstruction result was compared with the cross-section dimensions by calibrated SEM and TEM, and a minor error was identified. It is confirmed that the measurement bias of the CD measurement of the tested micro grating can be controlled to be within 1.0 nanometers. The remaining deviations may be potentially contributed to several possible factors in AFM measurement. As seen in the tested results, the significant difference identified may have been contributed to inaccurate diameter estimation of the AFM tip. For this reason, a more accurate method to identify the profile of the AFM tip is required for higher CD measurement accuracy to be further achieved.

ACKNOWLEDGMENT

Financial support for this work was provided by the National Science Council Taiwan, R.O.C, under the contract MOST 111-2218-E-002-031 and MOST 110-2221-E-002 -120 -MY3.

REFERENCES

Akca, D., *Matching of 3D surfaces and their intensities.* ISPRS Journal of Photogrammetry and Remote Sensing, 62(2): p. 112-121 (2007).

Bai, Z., et al., Narrow-linewidth laser linewidth measurement technology, Frontiers in Physics, Volume 9, id.684 (2021).

Bentley J. L., *Multidimensional binary search trees used for associative searching.* Communications of the ACM, 1975. 18(9): p. 509-517 (1975).

Besl, P. J., and McKay, N. D., *Method for registration of 3-D shapes. Sensor fusion IV: control paradigms and data structures.* SPIE (1992).

Canet-Ferrer, J. et al., Correction of the tip convolution effects in the imaging of nanostructures studied through scanning force microscopy, Nanotechnology, 3;25(39):395703 (2014).

Chen, Y. and Medioni, G., *Object modeling by registration of multiple range images.* Image and vision computing, 10(3): p. 145-155 (1992).

Dorai, C., Weng J. and Jain, A. K., *Optimal registration of object views using range data.* IEEE transactions on pattern analysis and machine intelligence, 19(10): p. 1131-1138 (1997).

Dahlen, G., et al. *Critical dimension AFM tip characterization and image reconstruction applied to the 45-nm node.* in *Metrology, Inspection, and Process Control for Microlithography XX*. SPIE (2006).

Finkel, R. A. and Bentley J. L., *Quad trees a data structure for retrieval on composite keys.* Acta informatica, 4(1): p. 1-9 (1974).

Fitzgibbon, A. W., *Robust registration of 2D and 3D point sets.* Image and vision computing, 21(13-14): p. 1145-1153 (2003).

Gruen, A., and Akca, D., *Least squares 3D surface and curve matching.* ISPRS Journal of Photogrammetry and Remote Sensing, 59(3): p. 151-174 (2005).

Giessibl, F.J., *Advances in atomic force microscopy.* Reviews of modern physics, 75(3): p. 949 (2003).

Heath, G.R., Kots, E., Robertson, J.L. et al. Localization atomic force microscopy. Nature 594, 385–390 (2021).

Huber, D. F. and Hebert, M., *Fully automatic registration of multiple 3D data sets.* Image and Vision Computing, 21(7): p. 637-650 (2003).

Jackins, C. L. and Tanimoto, S. L., *Oct-trees and their use in representing three-dimensional objects.* Computer Graphics and Image Processing, 14(3): p. 249-270 (1980).

Kleinknecht, H. P. and Meier, H., Linewidth measurement on IC masks and wafers by grating test patterns, Appl. Opt. 19, 525-533 (1980)

Masuda, T. and Yokoya, N., *A robust method for registration and segmentation of multiple range images.* Computer vision and image understanding, 61(3): p. 295-307 (1995).

Omohundro, S. M., *Five balltree construction algorithms.*: International Computer Science Institute Berkeley (1989).

Lang, K., et al., *Conducting atomic force microscopy for nanoscale tunnel barrier characterization.* Review of scientific instruments, 2004. 75(8): p. 2726-2731.

Liu, T., et al., *New algorithms for efficient high-dimensional nonparametric classification.* Journal of Machine Learning Research, 7(6) (2006).

Pottmann, H., Leopoldseder, S. and Hofer, M., *Registration without ICP.* Computer Vision and Image Understanding, 95(1): p. 54-71 (2004).

Sharp, G. C., Lee, S. W., and Wehe, D. K., *ICP registration using invariant features.* IEEE Transactions on Pattern Analysis and Machine Intelligence, 24(1): p. 90-102 (2002).

Vekinis, A. A. and Constantoudis, V., Quantifying geometric tip-sample effects in AFM measurements using certainty graphs, Micro and Nano Engineering, Vol. 8, 100067 (2020)

Sproull, R. F., *Refinements to nearest-neighbor searching ink-dimensional trees.* Algorithmica, 6(1): p. 579-589 (1991).

Yianilos, P. N., *Data Structures and Algorithms for Nearest Neighbor*. in *Proceedings of the fourth annual ACM-SIAM Symposium on Discrete algorithms*. SIAM (1993).

Zhang, Z., *Iterative point matching for registration of free-form curves and surfaces.* International journal of computer vision, 13(2): p. 119-152. (1994)

運用多視角原子力顯微鏡影像縫合技術於精密微線寬關鍵尺寸量測

陳亮嘉 阮方泰
國立台灣大學 機械工程學系

何柏青
工業技術研究院 量測技術中心

摘 要

本文提出一種嶄新的關鍵尺寸測量方法，採用原子力顯微鏡之多視圖掃描的影像疊合算法，來準確重建與量測微光柵的線寬。方法中運用嶄新之多視圖掃描和影像疊合演算法進行精確數據之融合，以精確重建標準光柵之線寬。由 SEM 以及 TEM 之實測數據證實，對於線寬為 820.1 nm 的光柵，AFM 測量微光柵的測量偏差(bias)可以控制在 1.0 nm 以下。